

In Situ Structural Characterization of Platinum Dendrimer-Encapsulated Oxygen Reduction Electrocatalysts

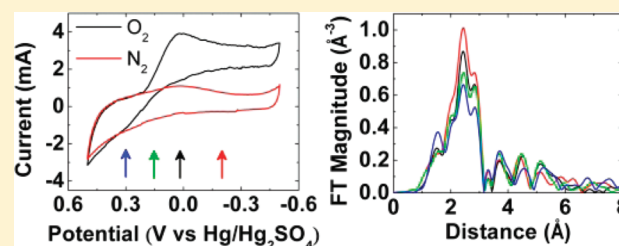
V. Sue Myers,[†] Anatoly I. Frenkel,^{*,‡} and Richard M. Crooks^{*,†}

[†]Department of Chemistry and Biochemistry, Center for Electrochemistry, Texas Materials Institute, Center for Nano- and Molecular Science and Technology, The University of Texas at Austin, 1 University Station, A5300, Austin, Texas 78712-0165, United States

[‡]Department of Physics, Yeshiva University, 245 Lexington Avenue, New York, New York 10016, United States

Supporting Information

ABSTRACT: In situ electrochemical extended X-ray absorption fine structure (EXAFS) was used to evaluate the structure of Pt dendrimer-encapsulated nanoparticles (DENs) during the oxygen reduction reaction (ORR). The DENs contained an average of just 225 atoms each. The results indicate that the Pt coordination number (CN) decreases when the electrode potential is moved to positive values. The results are interpreted in terms of an ordered core, disordered shell model. The structure of the DENs is not significantly impacted by the presence of dioxygen, but other electrogenerated species may have a significant impact on nanoparticle structure.



INTRODUCTION

Here, we report on the structural evolution of Pt dendrimer-encapsulated nanoparticles (DENs) containing ~ 225 atoms during the electrocatalytic oxygen reduction reaction (ORR). Our findings are based on in situ electrochemical extended X-ray absorption fine structure (EXAFS) measurements, which probe the local coordination environment of the Pt electrocatalyst. There are two important outcomes of these experiments. First, the Pt coordination number (CN) decreases when the electrode potential is moved to positive values, which is most likely due to disordering of the Pt at the particle surface. Furthermore, the particles show evidence of disorder at potentials in the double-layer region. Second, ligand effects on the structure of the Pt nanoparticle arising from dioxygen are minimal, although other electrolytic species may have a significant effect.

DENs are usually synthesized using a two-step procedure.¹ First, metal ions are sequestered within the interior of dendrimer templates. Second, addition of a chemical reducing agent, such as BH_4^- , yields zerovalent particles encapsulated within the dendrimer interior. Because this is a template synthesis, the size and chemical composition of DENs can be controlled to yield nanoparticles in the size range of <1 nm to ~ 3 nm.^{1–11} Multimetallic nanoparticles, including those having core@shell and alloy structures, can also be prepared by this route.¹ DENs are well-suited for studying fundamental aspects of catalysis because of their uniform size, structure, and composition, and because the dendrimer shell prevents agglomeration without passivating the metal surface.^{12,13} The small size of DENs (40–250 atoms) makes them particularly well-suited for studying catalytic reactions using in situ EXAFS. This is because EXAFS measures the average coordination environment of a material, and small particles, such as DENs,

possess a high ratio of surface atoms to interior atoms. Therefore, interactions between the surface of the DEN and reactants and products that might influence its structure can be easily observed. For larger particles, the CNs of the reactive surface atoms will be overwhelmed by the much greater signal arising from interior atoms.

We have previously reported two in situ electrochemical EXAFS studies of DENs.^{14,15} In one case, Pt DENs containing ~ 240 atoms were characterized during electrochemical CO adsorption and oxidation.¹⁴ The results indicated that CO adsorbs to the DEN surface, but that no significant degree of nanoparticle restructuring takes place before, during, or after adsorption. In the second study, we examined the underpotential deposition (UPD) of Cu onto Pt DENs.¹⁵ The core@shell structure of these materials was confirmed by analysis of the CN of each metal species. A key result of this study was that UPD layer of Cu did not affect the calculated CN of the Pt core. In other words, both of these studies indicated that ligand adsorption (CO in one case, and Cu in the other) has little or no effect on the structure of the Pt DENs. This is an important finding, because it suggests that DENs are relatively insensitive to surface processes and hence may be good experimental catalyst models for comparison to theoretical calculations.

In addition to our own work with DENs, there have been a number of other in situ EXAFS studies of Pt nanoparticles synthesized by more traditional means.^{16–28} Most of these have been focused on Pt oxide formation under steady-state conditions.^{16–25} A decrease in the Pt–Pt CN (n_{PtPt}) and an increase in the Pt–O CN (n_{PtO}) are typically observed when

Received: September 25, 2011

Revised: December 11, 2011

Published: January 5, 2012

the electrode potential is moved from the Pt double-layer region¹⁴ (where the ORR is active) to more positive potentials where the ORR is not active. However, one study reported no change in n_{Pt} over this same potential range.¹⁶ In general, the magnitude of the change in n_{Pt} and n_{PtO} is dependent on particle size, with smaller particles exhibiting greater changes in CN.^{17–28} As discussed earlier, this is primarily because a higher fraction of atoms reside on the surface of smaller particles.

Recently, several groups have reported in situ studies of proton exchange membrane fuel cells (PEMFCs) incorporating Pt nanoparticle ORR catalysts.^{29–32} All of these studies utilized a two-electrode configuration incorporating a Pd anode and a cathode composed of Pt/C catalyst dispersed on a carbon support. The results obtained from these studies vary considerably and in some instances the conclusions are inconsistent.

In the present paper, we observed that the effect of ligands (dioxygen species) on Pt DENs is minimal during the ORR, but that other electrolytic species may have a significant impact on DEN structure. Additionally, a reversible decrease in n_{Pt} was measured as a function of increasing potential above -0.20 V. We propose a model of increasing surface disorder beginning at or below a potential of -0.20 V.

EXPERIMENTAL SECTION

DEN Synthesis. Sixth-generation, hydroxyl-terminated poly(amidoamine) (PAMAM) dendrimers (G6-OH) in methanol were purchased from Dendritech, Inc. (Midland, MI). The methanol was removed by vacuum evaporation prior to use and a $100.0 \mu\text{M}$ aqueous stock solution was prepared from the dried powder. Sufficient 0.10 M K_2PtCl_4 (Sigma-Aldrich) was added to an aqueous solution of G6-OH so that the ratio of Pt^{2+} :G6-OH was 225:1 and the final concentration of G6-OH was $10.0 \mu\text{M}$. This solution was allowed to react for 72 h, after which 10 mol equiv (relative to the total metal content) of freshly prepared NaBH_4 was added. The resulting solution was tightly capped and allowed to react for an additional 22 h. Next, the Pt DEN solution was dialyzed into 4 L of water for 24 h using a 12.0 kDa cutoff dialysis sack (Sigma Aldrich). All aqueous solutions were prepared using $18 \text{ M}\Omega\text{-cm}$ Milli-Q water (Millipore, Bedford, MA).

DEN Characterization. UV-vis absorbance spectra were collected before and after chemical reduction using a Hewlett-Packard HP8453 spectrometer and a 1.00 mm path-length quartz cuvette. A solution of $10.0 \mu\text{M}$ aqueous G6-OH was used for the blank. All spectra were consistent with previously published reports for Pt DENs of this size.^{15,33}

Micrographs obtained by transmission electron microscopy (TEM) were collected using a JEOL-2010F TEM operating at 200 kV in transmission mode. TEM grids were prepared by dropping several microliters of the DEN solution onto a carbon-coated, 400-mesh Cu grid (EM Sciences) and drying in air. The average diameter of the Pt DENs used in this study, $1.8 \pm 0.3 \text{ nm}$, was determined by measuring 100 individual particles. This size is consistent with previously published results.^{14,15,33,34}

Electrochemistry. Electrochemical experiments were performed using either a glassy carbon electrode (GCE) and a standard three-electrode cell, or a carbon-paper electrode (Avcarb75, Ballard Power Systems, Inc.) and a spectroelectrochemical cell. The counter electrode was a glassy carbon chip and the reference electrode was $\text{Hg}/\text{Hg}_2\text{SO}_4$. All potentials are reported relative to the $\text{Hg}/\text{Hg}_2\text{SO}_4$ reference electrode. High purity LiClO_4 (99.99%, Aldrich), HClO_4 (Ultrapure, JT Baker), and H_2SO_4 (Trace metal grade, Fisher) were used as supporting electrolytes. A CHI 700d bipotentiostat (CH Instruments, Austin, TX) was used for experiments carried out in the three-electrode cell. The GCE was polished sequentially with 1.0, 0.3, and $0.05 \mu\text{m}$ alumina particles, and then sonicated in water for several minutes prior to use. Details of the immobilization of the DENs onto the GCE are given in the Results and Discussion section. For in situ

EXAFS electrochemical measurements, a portable Pine WaveNow potentiostat (Pine Research Instrumentation, Grove City, PA) was used. The carbon-paper electrode was cycled between 1.50 and -1.50 V in 0.5 M H_2SO_4 before immobilization of the DENs. Additional information about DEN immobilization onto the carbon-paper electrode is also provided in the Results and Discussion section.

Spectroelectrochemical Cell. We previously reported on the design of a three-electrode, in situ, X-ray absorption spectroscopy (XAS) cell.^{14,15} A similar cell design was utilized here. Briefly, the cell consists of two Teflon pieces that are clamped together to form an electrolyte reservoir. A window in the cell allows the X-ray beam to pass through the working electrode, and Kapton tape is used to seal the window. Ports are provided for reference and counter electrodes, as well as for gas sparging. A photograph of the cell and further details about the cell design are provided in the Supporting Information.

X-ray Absorption Spectroscopy. XAS data were collected using beamline X18B at the National Synchrotron Light Source (NSLS) at the Brookhaven National Laboratory (BNL) in New York (USA). The L_3 absorption edge spectra of Pt were measured in fluorescence mode by orienting the electrode at 45° relative to the beam. A five-grid Lytle detector filled with Ar gas was used for fluorescence detection, and Soller slits and a Zn filter were used to minimize scattering. Between 2 and 6 energy scans using 3.0 s integration times were averaged to improve the signal-to-noise ratio of the EXAFS spectra. Pt foil reference spectra were collected concurrently with the DENs spectra and used for energy calibration. The data were analyzed using the IFEFFIT software package and FEFF6 program.^{35,36}

RESULTS AND DISCUSSION

Pt DEN Synthesis. Complete information about the synthesis of Pt DENs is provided in the Experimental Section, but, briefly, they are synthesized and prepared for electrocatalytic studies using the following three-step procedure. First, an appropriate, stoichiometric amount of PtCl_4^{2-} is added to an aqueous dendrimer solution. This results in complexation between Pt^{2+} and tertiary amine groups present within the dendrimer interior.^{33,37} Second, an excess of BH_4^- is added to the Pt^{2+} -dendrimer complex to reduce Pt^{2+} to zerovalent Pt. However, we have previously shown that reduction of Pt^{2+} is not complete under these conditions.^{14,33} Instead, a bimodal product distribution results, consisting of fully reduced nanoparticles and unreduced Pt^{2+} -dendrimer complex.³³ Third, the Pt DENs are dialyzed to remove reaction byproducts. Note that dendrimer-bound Pt^{2+} that remains unreduced after addition of BH_4^- can be fully reduced after electrode immobilization by applying a sufficiently negative electrode potential.¹⁴

Ex Situ Characterization. The Pt DENs were characterized using UV-vis spectroscopy, TEM, and cyclic voltammetry. Absorbance spectra and a representative TEM micrograph and size-distribution histogram are provided in the Supporting Information. The Pt DEN system has been studied extensively, and the results obtained here are consistent with those published previously.^{14,15,33,34,38,39}

The Pt DENs were characterized electrochemically using a standard three-electrode cell and a polished GCE working electrode. Immobilization of the DENs onto the GCE was achieved using a previously published method.⁴⁰ Briefly, the electrode was immersed in an aqueous solution containing $10.0 \mu\text{M}$ G6-OH(Pt_{225}) and 0.10 M LiClO_4 , and the potential was cycled 3 times between -0.20 and 0.70 V. Next, the GCE was rinsed and transferred to a 0.10 M HClO_4 electrolyte solution. Finally, the electrode was cycled between 0.60 V and -0.60 V to reduce any Pt^{2+} that might be present within the dendrimers,¹⁴ and to clean the surfaces of the DENs.

Figure 1 is a cyclic voltammogram (CV) of the immobilized G6-OH(Pt₂₂₅) DENs. It reveals the characteristic features of Pt

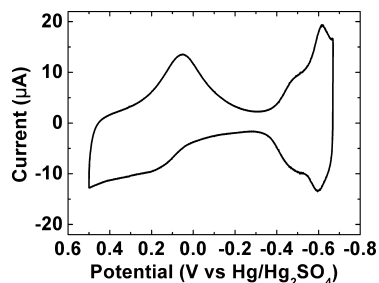


Figure 1. Cyclic voltammogram obtained using a GCE modified with G6-OH(Pt₂₂₅) DENs. The scan rate = 100 mV/s, the electrode area = 7.1 mm², and the electrolyte solution was 0.10 M HClO₄ sparged with N₂.

electrochemistry:¹⁴ oxidation of Pt at potentials positive of 0.20 V, an oxide reduction peak centered at 0.10 V, and a series of peaks present at potentials negative of -0.40 V that arise from the adsorption and desorption of H atoms on different crystallographic facets of the DEN surfaces. The total surface area of Pt was determined by measuring the charge arising from hydrogen adsorption, and then converting this value to surface area using the accepted charge density value for hydrogen adsorption on bulk, polycrystalline Pt of 210 µC/cm².^{15,34} The experimentally determined surface area (0.12 cm²) can be compared with an estimated surface area (0.05 cm²) calculated using assumptions we have discussed previously.³⁴ Given the approximate nature of the assumptions involved in this calculation and the conversion of measured charge to surface area, these values are in reasonable agreement.

Immobilization of DENS onto Avcarb75. A commercial carbon-paper electrode, Avcarb75, was used as the working electrode for in situ EXAFS measurements. Immobilization of Pt DENs onto Avcarb75 was achieved using a previously published method.^{14,41} Briefly, an electrochemical pretreatment of the carbon-paper electrode in sulfuric acid was performed to improve wetting of the electrode material (a photograph illustrating this effect is provided in the Supporting Information). Next, the carbon paper was rinsed and immersed in a Pt DEN solution for 12 h. Finally, a CV (Figure 2) was

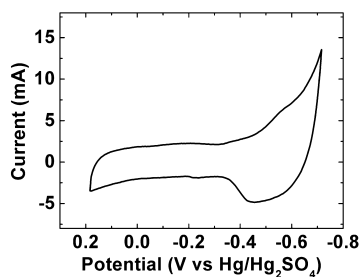


Figure 2. Cyclic voltammogram obtained using an Avcarb75 carbon-paper electrode modified with G6-OH(Pt₂₂₅) DENs. The data were collected in a standard three-electrode cell. The scan rate = 10 mV/s, the electrode area = 6.5 cm², and the electrolyte solution was 0.10 M HClO₄ sparged with N₂.

obtained in the H-atom adsorption/desorption potential region to ensure the presence of G6-OH(Pt₂₂₅) DENs on the electrode surface. Note that this CV is somewhat different

from the one obtained using the GCE (Figure 1). This is because the surface area and resistance of Avcarb75 is greater than that of the GCE, leading to significantly increased capacitance and poorly resolved hydrogen peaks.

After trimming the Pt DEN-modified Avcarb75 working electrode and placing it into the spectroelectrochemical cell, the electrode was held at -0.70 V while sparging the electrolyte solution with N₂. As mentioned earlier, this step completes the reduction of Pt²⁺ that might be present within the dendrimers¹⁴ and cleans the surface of the DENs. Figure 3 shows X-ray

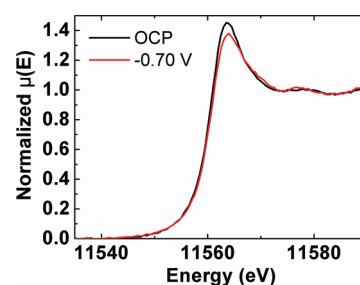


Figure 3. XANES spectra of G6-OH(Pt₂₂₅) at the OCP and at -0.70 V collected in the spectroelectrochemical cell using 0.10 M HClO₄ electrolyte solution. The decrease in the white line intensity indicates reduction of Pt²⁺ after application of the negative potential.

absorption near edge structure (XANES) spectra collected at the open circuit potential (OCP, black trace) before placing the working electrode under potential control and after applying a potential of -0.70 V (red trace). There is a noticeable decrease in the white line region of the spectrum after application of the negative potential, indicating a lower oxidation state of Pt and hence reduction of residual intradendrimer Pt²⁺.²³

In Situ ORR Experiments. Figure 4 shows CVs obtained using the spectroelectrochemical cell and a G6-OH(Pt₂₂₅)-

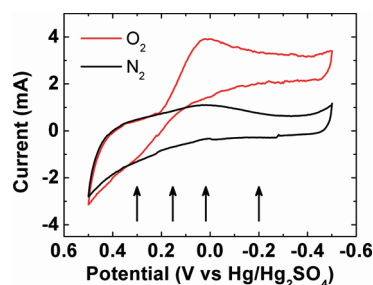


Figure 4. Cyclic voltammograms obtained using an Avcarb75 carbon-paper electrode modified with G6-OH(Pt₂₂₅) DENs. The arrows indicate the potentials at which XAS spectra were collected. Both the voltammograms and XAS data were obtained using the spectroelectrochemical cell shown in Figure S1 (Supporting Information). The scan rate = 10 mV/s, the electrode area = 3.6 cm², and the electrolyte solution was 0.10 M HClO₄ sparged with O₂ or N₂, as indicated in the legend.

modified electrode in the presence (red) and absence (black) of O₂. The arrows in Figure 4 indicate the potentials at which EXAFS spectra were collected: -0.20, 0.05, 0.15, and 0.30 V. Note that the currents in these CVs are lower than in the CV shown in Figure 2. This is because the area of the Avcarb75 electrode was reduced in size before placing it into the spectroelectrochemical cell.

EXAFS were data collected with the working electrode held at the desired potential while the electrolyte was sparged with either N_2 or O_2 . In some cases, the electrode was held at a particular potential for several hours so that multiple EXAFS scans could be collected to improve the signal-to-noise ratio of the spectra. Figure 5 is a plot of current vs time for each of the

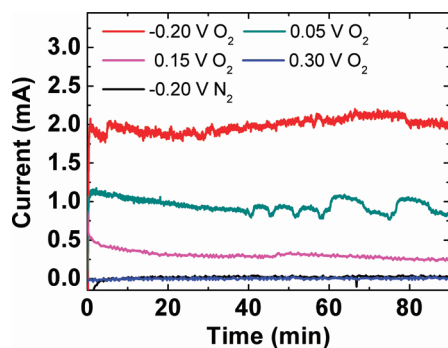


Figure 5. Plots of current vs time obtained while the G6-OH(Pt₂₂₅)-modified Avcarb75 electrode was held under electrochemical control at the potentials indicated in the legend. Data collection was initiated ($t = 0$) as soon as the potential was applied, and EXAFS data collection began at $t = 30$ min. Only the first 90 min of data collection are shown here, but the complete plots are provided in Figure S5 (Supporting Information). The 0.10 M HClO₄ electrolyte solution was sparged with O_2 or N_2 , as indicated in the legend. The electrode area was 1.6 cm².

four potentials indicated in Figure 4. Current data collection began immediately upon application of the indicated electrode potential ($t = 0$) and XAS data collection began at $t = 30$ min (to ensure steady-state conditions). The complete current-vs-time plots are provided in the Supporting Information. Fluctuations in the currents, which are most apparent in the green trace, are most likely due to bubble formation or irregular convection patterns in the cell caused by slight changes in gas flow.

In Situ XAS. The black EXAFS spectrum in Figure 6 was collected while the DEN-modified electrode was held at 0.15 V

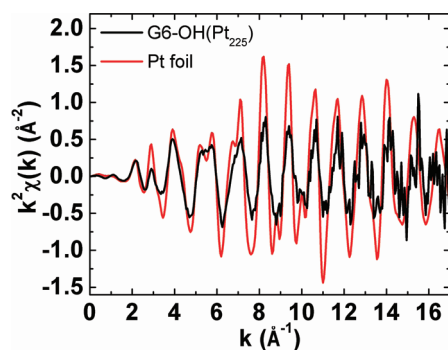


Figure 6. The black trace is a representative EXAFS spectrum (Pt L₃ edge) obtained from a G6-OH(Pt₂₂₅)-modified Avcarb75 electrode held at a potential of 0.15 V in 0.10 M HClO₄ sparged with O_2 . The red trace is a spectrum of a Pt foil. EXAFS spectra obtained under other conditions are provided in Figure S6 of the Supporting Information.

in 0.10 M HClO₄ sparged with O_2 . The red spectrum was obtained from a Pt foil collected on the same beamline. EXAFS spectra obtained under other conditions are provided in the

Supporting Information. All spectra exhibit decreased amplitudes relative to the bulk Pt, which is characteristic of nanoparticles.⁴² The data were fit using k windows that began at 3 Å⁻¹ and extended to values between 12 and 15 Å⁻¹, depending on the noise present in each spectrum at high k . For example, the data shown in Figure 6 were fit from $k = 3$ –12.5 Å⁻¹. The complete set of k windows used to fit all the EXAFS spectra, along with the R_{bkg} and R window values, are provided in the Supporting Information. To eliminate multiple-scattering effects and minimize the number of variables in the fit model, only the first Pt–Pt and Pt–O coordination shells were used for each spectrum. The best model was chosen on a sample-by-sample basis, as determined by the statistical fit parameters and by visual agreement of the experimental spectra and fit results. A multiple-scattering analysis of the sample at -0.20 V with N_2 sparging was also performed, as discussed in the following section.

Figure 7 shows the Pt–Pt (n_{PtPt} (black) and n_{PtO} (red), respectively) for each experiment. CNs determined

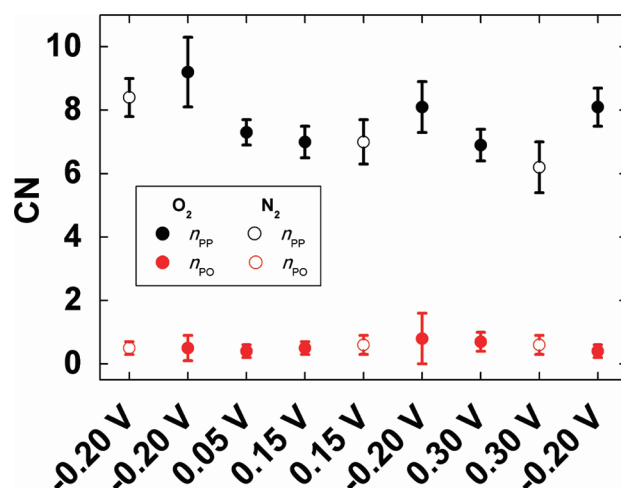


Figure 7. Pt–Pt (n_{PtPt}) and Pt–O (n_{PtO}) coordination numbers, determined from fits to the EXAFS data, as a function of electrode potential for G6-OH(Pt₂₂₅) DENs. Data were obtained using a 0.10 M HClO₄ electrolyte solution sparged with either N_2 or O_2 . The potentials are given in the order of data collection.

for Pt DENs in the presence of O_2 and N_2 are represented by filled and empty circles, respectively. The data are plotted in the order collected, beginning with the most reducing potential (-0.20 V) and continuing to the most positive potential (0.30 V). Several replicate data points were collected at -0.20 V under O_2 sparging to ensure that differences in CNs arise from electrode potential changes rather than drift or other irreversible effects. The results in Figure 7 as well as the values obtained for other important fitting parameters are presented in numerical form in Table 1.

Several observations can be drawn from Figure 7. First, there is a significant increase in n_{PtPt} at more negative potentials in the presence of both O_2 and N_2 . At -0.20 V, the most reducing potential considered in this study, n_{PtPt} is between 8 and 9.2. This is somewhat lower than the theoretical n_{PtPt} (9.5) for a 225-atom fcc truncated octahedral particle. However, when multiple-scattering analysis and electron microscopy measurements are taken into account, the EXAFS results are consistent with the nominal 225-atom clusters (vide infra). Previous studies with Pt DENs demonstrated n_{PtPt} greater than or equal

Table 1. Fit Values Obtained from EXAFS Simulations

	n_{PtPt}	n_{PtO}	R_{PtPt} (Å)	σ_{PtPt}^2 (Å ²)	ΔE_0 (eV)	R_{PtO} (Å)	σ_{PtO}^2 (Å ²)
N_2							
0.30 V	6.2(8)	0.6(3)	2.752(7)	0.0062(4)	8.6(7)	0.006(16)	0.000(3)
0.15 V	7.0(7)	0.6(3)	2.748(5)	0.0064(6)	8.2(7)	0.021(19)	0.003(5)
−0.20 V	8.4(6)	0.5(2)	2.747(3)	0.0066(9)	7.9(1.2)	0.055(16)	0.000(4)
O_2							
0.30 V	6.9(5)	0.7(3)	2.751(4)	0.0064(5)	8.6(8)	0.017(14)	0.003(4)
0.15 V	7.0(5)	0.5(2)	2.745(4)	0.0060(5)	8.0(8)	0.019(15)	0.001(4)
0.05 V	7.3(4)	0.4(2)	2.734(3)	0.0062(4)	7.6(6)	0.009(14)	0.001(4)
	9.2(1.1)	0.5(4)	2.745(7)	0.0067(8)	8.5(1.2)	0.015(33)	0.003(9)
−0.20 V	8.1(8)	0.8(8)	2.747(6)	0.0060(7)	8.4(1.1)	0.025(38)	0.011(15)
	8.1(6)	0.4(2)	2.740(3)	0.0058(3)	7.1(7)	0.010(17)	0.000(3)

to the predicted values at an even more reducing potential (−0.70 V) under similar conditions.¹⁴ This is consistent with the trend observed here for the CN to increase at more negative potentials. Second, there is no significant difference between n_{PtPt} and n_{PtO} collected in the presence of O_2 and the N_2 . However, as indicated in Table 1, there may be a systematic effect of increased Pt–Pt bond lengths (R_{PtPt}) under N_2 sparging. Finally, the changes in the coordination environments of the particles under potential control appear to be largely reversible (compare the values of n_{PtPt} at −0.20 V in Table 1).

Multiple-Scattering Analysis. Previous studies have shown that the CNs of multiple-scattering contributions to EXAFS data in small nanoparticles can be used to distinguish between different particle geometries.^{42–46} A multiple-scattering fit of the EXAFS spectra collected while the DENs were held under the most reducing potential (−0.20 V) was performed to characterize the size and shape of the particles. Figure 8 shows the Fourier-transformed EXAFS spectra and the

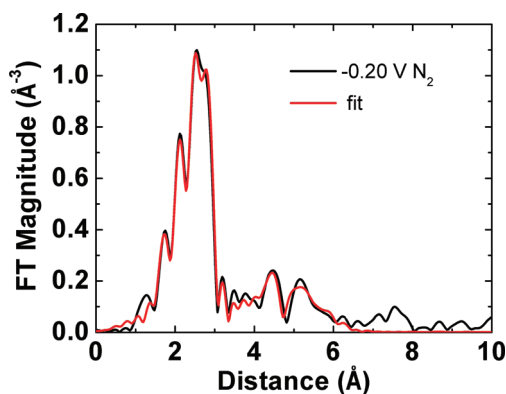

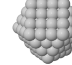
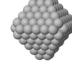


Figure 8. Fourier transformed EXAFS spectrum obtained from (black trace) a G6-OH(Pt₂₂₅)-modified Avcarb75 electrode held at a potential of −0.20 V in 0.10 M HClO₄ sparged with N_2 . The red trace is the multiple-scattering fit to these data. The k and R windows for this analysis were 2.5–14 Å^{−1} and 1.30–6.31 Å, respectively, and $R_{\text{bkg}} = 1.3$ Å.

multiple-scattering analysis of the Pt DENs measured at −0.20 V while sparging with N_2 . Table 2 compares the predicted CNs for several types of fcc clusters to the values obtained from the multiple-scattering fit. The effective diameters of the model clusters and the average diameter of the particles (as determined by TEM) are also included in the table. The experimental CNs and TEM data are consistent with a model of small, quasi-spherical clusters, although the observed first nearest neighbor (1NN) CNs are smaller than the model

Table 2. Coordination Numbers for fcc Cluster Models and Experimental Results for Multiple-Scattering Fit Analysis of the Data Collected at −0.20 V under N_2 Sparging

	140 atoms D=1.5 nm	147 atoms D=1.7 nm	225 atoms D=2.0 nm	Experiment D=1.8±0.3 nm
				
N1	9.1	9.0	9.5	8.4±0.4
N2	3.6	4.0	3.8	3.3±2.3
N3	13.4	13.1	14.7	20.1±7.7
N4	6.2	6.1	7.0	6.0±2.3
NO	--	--	--	0.4±0.1

values. This is consistent with previous comparative studies of TEM and EXAFS data.⁴⁷ Further discussion of this observation is given below. Interpretation of the multiple-scattering fit analysis for Pt DENs held at potentials greater than −0.20 V is more complicated due to larger number of possible models, and therefore our discussion is limited to this single potential.

Analysis of the Results. Guided by the combination of the in situ EXAFS results and the ex situ TEM data, we will propose the most plausible scheme for structural transformations that occur in the Pt DENs at different potentials. We will review several possible scenarios and discuss how they compare with relevant data.

Certain models are consistent with the observation of a decreasing n_{PtPt} with increasing potential and, yet, should be discounted as inconsistent with other information about the system. For instance, dissolution of the Pt atoms from the particles will result in smaller nanoparticles and free, uncoordinated (or, alternatively, polymer- or oxygen- or hydroxocomplex-bound) Pt atoms or ions, thereby lowering n_{PtPt} .⁴⁸ However, such dissolution would likely result in irreversible changes to n_{PtPt} . Additionally, the reduction of n_{PtPt} caused by dissolution should be accompanied by even greater reduction in the contribution from the higher-order coordination shells. Indeed, let us assume for simplicity that all 225-atom clusters decomposed into identical small particles with CNs between 6 and 7 (Table 1). These CNs correspond to closed shell clusters of ~13 atoms (considering icosahedral clusters).⁴⁴ In such clusters, the EXAFS signal originating from higher-order shells will be inconsistent with our experimental data.⁴⁹ Figure 9 plots selected Fourier-transformed EXAFS spectra. The peak marked with the arrow corresponds primarily to second-shell coordination. As previously shown both theoretically⁴⁴ and experimentally,⁴⁹ this peak should be absent

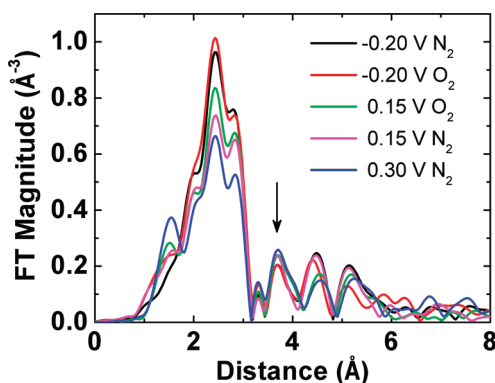


Figure 9. Fourier transformed EXAFS spectra. All data shown have an R_{bkg} of 1.3 Å and a k range of 3–12 Å⁻¹.

in icosahedral 13-atom clusters. For the close-packed 13-atom clusters, a second peak is present in the FT data,⁴⁹ but the 1NN CN is too low (5.54) compared to our experimental data (Table 1).

Another possible explanation for a decrease in n_{PtPt} with increasing potential is the formation of surface oxides.²⁵ Oxidation of the surface will reduce the CN in two ways. First, if PtO_n forms on the surface of the particles, it may disrupt Pt–Pt metal bonding thereby lowering the ensemble-average CN for Pt metal. For small clusters, any surface defect (adatom or vacancy) will significantly reduce cluster-average CN. Second, recent studies have shown that increased asymmetric disorder (caused by, for example, ligand-induced strain)⁵⁰ in nanoparticles relative to bulk materials leads to decreased apparent metal CNs in the nanoparticle systems.⁵¹ Accordingly, it would be possible for adsorption of electrochemically produced ligands to disrupt the first Pt shell without affecting the ordered metal core. These species could include electrogenerated oxygenated Pt intermediates,²⁵ which could be present even in the absence of O_2 (this is, under N_2 sparging conditions). Such disorder is inherently asymmetric and can lead to the apparent reduction in CN described above. Indeed, the surface atoms are mechanically under-constrained, and have more degrees of freedom than the interior atoms. Accordingly, their bond length distribution is different from that in the cluster interior and, hence, the ensemble average bond length distribution is bimodal. These effects cannot be resolved using present methods of EXAFS data analysis, but their presence is suggested by the results obtained conventionally.⁵⁰

As the surface disorder increases at increasingly higher potentials, the signal from higher order shells will become progressively less and less intense. Although a clear trend of decreasing multiple-scattering signal is not observed, the data are consistent with a model of increasing disorder at the higher potentials (Figure 9).

Given the discussion thus far, we propose an “ordered core-disordered shell” model. This model assumes that the nanoparticle surface is already partially disordered even at -0.20 V, and that it becomes further disordered as oxidation of Pt begins to occur. However, in this model, the Pt core remains relatively ordered at all potentials. The fact that the shell is always disordered explains why multiple-scattering contributions are relatively unaffected by changes to the electrode potential. Indeed, multiple-scattering contributions in an fcc structure are dominated by collinear Pt–Pt–Pt arrangements, and they decrease in proportion to the square of the bonding

angle when bonding disorder is present.^{52,53} Therefore, a large signal intensity in the high R -region, and, hence, the multiple-scattering contributions, should be dominated by the ordered core in such systems even for small angular disorder. Therefore, even as disorder increases, there is little additional effect on the multiple-scattering contribution. This model is supported by the multiple-scattering analysis described in the previous section (Table 2). Smaller-than-predicted CNs are observed for most shells at -0.20 V, although the diameter of the 225-atom, truncated octahedron model agrees with the TEM. This suggests the presence of disorder in the outermost DEN shell even at this potential.

It is important to mention that although this study provides evidence for surface disorder at potentials > -0.20 V, at even more reducing potentials the particles are clearly faceted. This is apparent from the well-defined hydrogen atom adsorption/desorption peaks present in Figure 1 at potentials < -0.4 V. This observation is fully consistent with the model described above, and it clearly shows that, even in DENs, which are not in direct contact with the electrode surface, the electrode potential has a significant influence on particle structure.

SUMMARY AND CONCLUSIONS

DENs are good model systems for studying catalytic processes using EXAFS because of their well-defined structural properties and high proportion of surface atoms relative to fully coordinated atoms. That is, because $\sim 65\%$ of the atoms in a $\text{G6-OH}(\text{Pt}_{225})$ particle are predicted to be at the surface, the effects of reaction intermediates on the surface atoms of DENs are observable in EXAFS.

The principal finding to emerge from the present study is that the Pt–Pt CN is a function of the electrode potential. We interpreted this result in terms of a model in which only the surface Pt atoms are affected by the potential. This is interesting, because although the important role of surface strain in determining ORR reactivity has been previously demonstrated,⁵⁴ our results are among the first to confirm this correlation spectroscopically. We found that at strongly reducing potentials (< -0.4 V) the outer Pt shell is ordered, as evidenced by the presence of well-defined H-atom adsorption and desorption peaks in the voltammetry. However, as the potential is moved in the positive direction, into and past the double-layer potential region, increasing disorder is signaled by a reduction in the Pt–Pt CN observed by in situ EXAFS experiments. Such order/disorder transitions are likely to have a dramatic effect on electrocatalytic reactions, and therefore, we plan to look for this type of behavior in future studies.

One final point is worth mentioning. There is a fundamental difference between DENs and all other Pt nanoparticle systems that have been examined by EXAFS previously. Specifically, in the case of DENs, the nanoparticle is not in direct contact with the electrode surface. Rather, it is sequestered within the dendrimer a small distance away. Therefore, DENs provide a good model system for studying the effects of adsorbates and electrode potential in the absence of specific interactions exerted by the electrode surface. In other cases, substrate effects tend to have a strong influence on nanoparticle structure, and smaller effects driven by adsorbates or potential may be swamped out.

■ ASSOCIATED CONTENT

■ Supporting Information

Photograph of the spectroelectrochemical cell; UV-vis absorbance spectra of G6-OH(Pt²⁺)₂₂₅ and G6-OH(Pt₂₂₅); TEM micrograph of G6-OH(Pt₂₂₅) and a size-distribution histogram; photographs of carbon paper before and after an electrochemical pretreatment, current as a function of time during in situ EXAFS measurements; EXAFS spectra of Pt DENs for all potentials reported in the main text; and a table of EXAFS fitting parameters. This material is available free of charge via the Internet at <http://pubs.acs.org>.

■ AUTHOR INFORMATION

Corresponding Author

*R.M.C.: E-mail crooks@cm.utexas.edu; Voice 512-475-8674.
A.I.F.: E-mail anatoly.frenkel@yu.edu; Voice 212-340-7827.

■ ACKNOWLEDGMENTS

V.S.M. and R.M.C. gratefully acknowledge financial support from the U.S. Department of Energy, Office of Basic Energy Sciences (Grant No. DE-FG02-09ER16090). Sustained support from the Robert A. Welch Foundation (Grant F-0032) is also acknowledged. A.I.F. acknowledges support of the Department of Energy Grant No. DE-FG02-03ER15476. Use of the NSLS is supported by the U.S. Department of Energy, Office of Science, Office of Basic Energy Sciences, under Contract No. DE-AC02-98CH10886. Beamline X18B at the NSLS is supported in part by the Synchrotron Catalysis Consortium, U.S. Department of Energy Grant No. DE-FG02-05ER15688. We also thank Ji-Ping Zhou (Texas Materials Institute), and Nebojsa Marinkovic and Syed Khalid (NSLS), for assistance with TEM and beamline measurements, respectively.

■ REFERENCES

- (1) Myers, V. S.; Weir, M. G.; Carino, E. V.; Yancey, D. F.; Pande, S.; Crooks, R. M. *Chem. Sci.* **2011**, *2*, 1632–1646.
- (2) Zhao, M.; Sun, L.; Crooks, R. M. *J. Am. Chem. Soc.* **1998**, *120*, 4877–4878.
- (3) Lang, H.; May, R. A.; Iversen, B. L.; Chandler, B. D. *J. Am. Chem. Soc.* **2003**, *125*, 14832–14836.
- (4) Gröhn, F.; Bauer, B. J.; Akpalu, Y. A.; Jackson, C. L.; Amis, E. J. *Macromolecules* **2000**, *33*, 6042–6050.
- (5) Ozturk, O.; Black, T. J.; Perrine, K.; Pizzoloto, K.; Williams, C. T.; Parsons, F. W.; Ratliff, J. S.; Gao, J.; Murphy, C. J.; Xie, H.; Ploehn, H. J.; Chen, D. A. *Langmuir* **2005**, *21*, 3998–4006.
- (6) Singh, A.; Chandler, B. D. *Langmuir* **2005**, *21*, 10776–10782.
- (7) Alexeev, O. S.; Siani, A.; Lafaye, G.; Williams, C. T.; Ploehn, H. J.; Amiridis, M. D. *J. Phys. Chem. B* **2006**, *110*, 24903–24914.
- (8) Vijayaraghavan, G.; Stevenson, K. J. *Langmuir* **2007**, *23*, 5279–5282.
- (9) Huang, W.; Kuhn, J. N.; Tsung, C.-K.; Zhang, Y.; Habas, S. E.; Yang, P.; Somorjai, G. A. *Nano Lett.* **2008**, *8*, 2027–2034.
- (10) Yancey, D. F.; Carino, E. V.; Crooks, R. M. *J. Am. Chem. Soc.* **2010**, *132*, 10988–10989.
- (11) Pande, S.; Weir, M. G.; Zaccheo, B. A.; Crooks, R. M. *New J. Chem.* **2011**, Advance Article.
- (12) Niu, Y.; Yeung, L. K.; Crooks, R. M. *J. Am. Chem. Soc.* **2001**, *123*, 6840–6846.
- (13) Petkov, V.; Bedford, N.; Knecht, M. R.; Weir, M. G.; Crooks, R. M.; Tang, W.; Henkelman, G.; Frenkel, A. *J. Phys. Chem. C* **2008**, *112*, 8907–8911.
- (14) Weir, M. G.; Myers, V. S.; Frenkel, A. I.; Crooks, R. M. *ChemPhysChem* **2010**, *11*, 2942–2950.
- (15) Carino, E. V.; Crooks, R. M. *Langmuir* **2011**, *27*, 4227–4235.

- (16) Arruda, T. M.; Shyam, B.; Ziegelbauer, J. M.; Mukerjee, S.; Ramaker, D. E. *J. Phys. Chem. C* **2008**, *112*, 18087–18097.
- (17) Mukerjee, S.; McBreen, J. *J. Electroanal. Chem.* **1998**, *448*, 163–171.
- (18) Mukerjee, S.; Srinivasan, S.; Soriaga, M. P.; McBreen, J. *J. Phys. Chem.* **1995**, *99*, 4577–4589.
- (19) Sanjeev, M.; Supramaniam, S.; Manuel, P. S.; James, M. J. *Electrochem. Soc.* **1995**, *142*, 1409–1422.
- (20) Maniguet, S.; Mathew, R. J.; Russell, A. E. *J. Phys. Chem. B* **2000**, *104*, 1998–2004.
- (21) Lampitt, R. A.; Carrette, L. P. L.; Hogarth, M. P.; Russell, A. E. *J. Electroanal. Chem.* **1999**, *460*, 80–87.
- (22) Russell, A. E.; Maniguet, S.; Mathew, R. J.; Yao, J.; Roberts, M. A.; Thompsett, D. *J. Power Sources* **2001**, *96*, 226–232.
- (23) Teliska, M.; O'Grady, W. E.; Ramaker, D. E. *J. Phys. Chem. B* **2005**, *109*, 8076–8084.
- (24) Murthi, V. S.; Urian, R. C.; Mukerjee, S. *J. Phys. Chem. B* **2004**, *108*, 11011–11023.
- (25) Imai, H.; Izumi, K.; Matsumoto, M.; Kubo, Y.; Kato, K.; Imai, Y. *J. Am. Chem. Soc.* **2009**, *131*, 6293–6300.
- (26) Mathew, R. J.; Russell, A. E. *Top. Catal.* **2000**, *10*, 231–239.
- (27) Antolini, E.; Salgado, J. R. C.; Giz, M. J.; Gonzalez, E. R. *Int. J. Hydrogen Energy* **2005**, *30*, 1213–1220.
- (28) Russell, A. E.; Rose, A. *Chem. Rev.* **2004**, *104*, 4613–4636.
- (29) Tada, M.; Murata, S.; Asakoka, T.; Hiroshima, K.; Okumura, K.; Tanida, H.; Uruga, T.; Nakanishi, H.; Matsumoto, S.-i.; Inada, Y.; Nomura, M.; Iwasawa, Y. *Angew. Chem.* **2007**, *119*, 4388–4393.
- (30) Hudson, S. L.; Balla, S. C.; Blaney, K. B.; Chouchelamaneb, G. H.; Fiddy, S. G.; Harvey, I.; Sivasubramaniamb, P.; Tessiera, B. C.; Theobalda, B. R. C.; Thompsetta, D.; Russell, A. E. *ECS Trans.* **2008**, *16*, 1395–1404.
- (31) Principi, E.; Witkowska, A.; Dsoke, S.; Marassi, R.; Di Cicco, A. *Phys. Chem. Chem. Phys.* **2009**, *11*, 9987–9995.
- (32) Witkowska, A.; Principi, E.; Di Cicco, A.; Dsoke, S.; Marassi, R.; Olivi, L.; Centazzo, M.; Albertini, V. R. *J. Non-Cryst. Solids* **2008**, *354*, 4227–4232.
- (33) Knecht, M. R.; Weir, M. G.; Myers, V. S.; Pyrz, W. D.; Ye, H.; Petkov, V.; Buttrey, D. J.; Frenkel, A. I.; Crooks, R. M. *Chem. Mater.* **2008**, *20*, 5218–5228.
- (34) Ye, H.; Crooks, J. A.; Crooks, R. M. *Langmuir* **2007**, *23*, 11901–11906.
- (35) Ravel, B.; Newville, M. *J. Synchrotron Rad.* **2005**, *12*, 537–541.
- (36) Zabinsky, S. I.; Rehr, J. J.; Ankudinov, A.; Albers, R. C.; Eller, M. *J. Phys. Rev. B: Condens. Matter* **1995**, *52*, 2995.
- (37) Gu, Y.; Sanders, P.; Ploehn, H. J. *Colloids Surf., A* **2010**, *356*, 10–15.
- (38) Wales, C. H.; Berger, J.; Blass, S.; Crooks, R. M.; Asherie, N. *Langmuir* **2011**, *27*, 4104–4109.
- (39) Zhao, M.; Crooks, R. M. *Adv. Mater.* **1999**, *11*, 217–220.
- (40) Ye, H.; Crooks, R. M. *J. Am. Chem. Soc.* **2005**, *127*, 4930–4934.
- (41) Ledesma-García, J.; Escalante García, I. L.; Rodríguez, F. J.; Chapman, T. W.; Godínez, L. A. *J. Appl. Electrochem.* **2008**, *38*, 515–522.
- (42) Frenkel, A. I.; Hills, C. W.; Nuzzo, R. G. *J. Phys. Chem. B* **2001**, *105*, 12689–12703.
- (43) Frenkel, A. I. *J. Synchrotron Radiat.* **1999**, *6*, 293–295.
- (44) Glasner, D.; Frenkel, A. I. *XAFS13 Conference Proceedings* **2007**, *882*, 746–748.
- (45) Roldan Cuenya, B.; Frenkel, A. I.; Mostafa, S.; Behafarid, F.; Croy, J. R.; Ono, L. K.; Wang, Q. *Phys. Rev. B* **2010**, *82*, 155450.
- (46) Roldan Cuenya, B.; Croy, J. R.; Mostafa, S.; Behafarid, F.; Li, L.; Zhang, Z.; Yang, J. C.; Wang, Q.; Frenkel, A. I. *J. Am. Chem. Soc.* **2010**, *132*, 8747–8756.
- (47) Agostini, G.; Pellegrini, R.; Leofanti, G.; Bertinetti, L.; Bertarione, S.; Groppo, E.; Zecchina, A.; Lamberti, C. *J. Phys. Chem. C* **2009**, *113*, 10485–10492.
- (48) Frenkel, A. I. *Z. Kristallogr.* **2007**, *222*, 605–611.

- (49) Menard, L. D.; Xu, H.; Gao, S.-P.; Twisten, R. D.; Harper, A. S.; Song, Y.; Wang, G.; Douglas, A. D.; Yang, J. C.; Frenkel, A. I.; Murray, R. W.; Nuzzo, R. G. *J. Phys. Chem. B* **2006**, *110*, 14564–14573.
- (50) Guliamov, O.; Frenkel, A. I.; Menard, L. D.; Nuzzo, R. G.; Kronik, L. *J. Am. Chem. Soc.* **2007**, *129*, 10978–10979.
- (51) Yevick, A.; Frenkel, A. I. *Phys. Rev. B* **2010**, *81*, 115451.
- (52) Frenkel, A.; Stern, E. A.; Voronel, A.; Qian, M.; Newville, M. *Phys. Rev. Lett.* **1993**, *71*, 3485–3488.
- (53) Frenkel, A.; Stern, E. A.; Voronel, A.; Qian, M.; Newville, M. *Phys. Rev. B* **1994**, *49*, 11662–11674.
- (54) Strasser, P.; Koh, S.; Annayev, T.; Greeley, J.; More, K.; Yu, C.; Liu, Z.; Kaya, S.; Nordlund, D.; Ogasawara, H.; Toney, M. F.; Nilsson, A. *Nat. Chem.* **2010**, *2*, 454–460.